Interannual atmospheric torque and El Niño-Southern Oscillation: Where is the polar motion signal?

Steven L. Marcus, Olivier de Viron, Jean O. Dickey

Interannual atmospheric torque and El Niño–Southern Oscillation: Where is the polar motion signal?

Steven L. Marcus,[1] Olivier de Viron,[2] and Jean O. Dickey[1]

Received 3 March 2010; revised 19 July 2010; accepted 18 August 2010; published 11 December 2010.

[1] In this paper, we investigate the atmospheric excitation of polar motion (PM) associated with the El Niño–Southern Oscillation (ENSO) phenomenon. ENSO effects on length-of-day due to changes in the axial component of atmospheric angular momentum (AAM) have long been recognized, but identification of PM excitation with ENSO-induced equatorial AAM anomalies has proved more elusive. Here we use an appropriately modified form of the inverted barometer (IB) assumption to study ENSO-related atmospheric torques arising from pressure loading on the Earth's ellipsoidal bulge and mountains and from frictional wind stress over the Earth's land- and ocean-covered surface. The resulting dissipation torques, which accommodate adjustment of the oceanic mass distribution to time-variable atmospheric loading, are found to be small. The ellipsoidal torques have the largest amplitude, reflecting the order-of-magnitude discrepancy between the height departures of the Earth's bulge (~20 km) and its surface orography (~2 km). Because of relatively uniform pressure covariances with the Southern Oscillation Index over the continents for the largely land-based X component and the uniform IB response for the largely ocean-based Y component; however, the ENSO-related PM excitation arising from the ellipsoidal torques is reduced to an amplitude comparable with the sum of regional mountain torques from the individual continents. The largest of these are generated over Asia and Antarctica, arising from efficient coupling of ENSO-related surface pressure anomalies with large-scale orographic features. The geometrical mitigation of the ellipsoidal torques, classically expected to dominate equatorial AAM forcing, accounts for the lack of a detectable atmosphere-driven polar motion response to ENSO.

Citation: Marcus, S. L., O. de Viron, and J. O. Dickey (2010), Interannual atmospheric torque and El Niño–Southern Oscillation: Where is the polar motion signal?, *J. Geophys. Res.*, *115*, B12409, doi:10.1029/2010JB007524.

1. Introduction

[2] The Earth's rotation is not constant but undergoes small variations on a broad range of time scales. These fluctuations of Earth rotation are classically divided into three parts: the changes in orientation of the Earth's rotation axis in the inertial (i.e., sidereal) frame are referred to as precession and nutation, the variations of Earth orientation around this axis define the polar motion (PM), and the magnitude fluctuations of the Earth's rotation vector are studied as length-of-day (LOD) variations.

[3] The interaction of the solid Earth (i.e., crust and mantle) with its surrounding fluids (i.e., atmosphere, ocean, hydrology, and the molten outer core) is the major cause of the Earth's nontidal rotational variation. On decadal and longer time scales, the interaction between the core and the mantle creates variation of the LOD at the level of several milliseconds; the interaction with the atmosphere is responsible for nearly all the shorter-period variation of the LOD, with the ocean [see *Ponte and Stammer*, 2000] and hydrology [see *Chen et al.*, 2000] playing much smaller roles. Subdecadal polar motion is mainly driven by the ocean and atmosphere, with hydrology (groundwater variations) also playing a role. The precession-nutation motion is driven by the gravitational interaction between the Earth's equatorial bulge and the Moon, the Sun, and other planets; variations in the atmosphere and the ocean at near-diurnal time scales also induce similar motions of the Earth's rotation axis [see *de Viron et al.*, 2001a; *Marcus et al.*, 2004].

[4] The effect of the atmosphere and ocean on Earth rotation is classically investigated through the angular momentum budget of the Earth system: if it can be considered as isolated, i.e., if no external torque is acting on it, the angular momentum of the system is conserved. Any change of the angular momentum of the fluid layers would then be associated with an opposite change of the solid Earth's angular momentum, directly linked to its rotation [see for instance *Munk and MacDonald*, 1960; *Barnes et al.*, 1983]. The angular momentum is usually decomposed into two terms: a matter term associated with the corotation of the atmosphere

[1] Jet Propulsion Laboratory, California Institute of Technology, Pasadena, California, USA.
[2] University Paris Diderot and Institut de Physique du Globe de Paris (CNRS), Paris, France.

0148-0227/10/2010JB007524

and ocean with the Earth and a motion term associated with the winds and currents. In this study, we use another approach, the so-called torque approach, to directly address the effect of the atmosphere on the solid Earth's rotation by evaluating the interaction torque between them [cf. *Wahr*, 1982; *de Viron et al.*, 1999]. The major torque for the equatorial components is due to the atmospheric pressure acting on the Earth's bulge, partly compensated by the gravitational attraction of the associated hydrostatic mass field by the bulge. These two effects dominate the equatorial components of the atmospheric torque at diurnal and longer periods and will be referred to as ellipsoidal torque. As the orography is specified in terms of geopotential height, the mountain torque will automatically include the nonbulge gravitational torque [e.g., *Wahr*, 1982; *Barnes et al.*, 1983]. Consequently, the three torques, which affect the atmospheric angular momentum (AAM) budget, may be classified as the ellipsoidal (or bulge) torque and the (local) mountain and friction torques.

[5] It has been known for several years that the El Niño–Southern Oscillation (ENSO) phenomenon strongly affects the climate system and consequently atmosphere-ocean-solid Earth interactions [e.g., *Chao*, 1989; *Dickey et al.*, 1992]. In particular, LOD is strongly affected by the ENSO cycle, the day being longer than usual during a (warm) El Niño event and shorter during a (cold) La Nina event [e.g., *Rosen et al.*, 1984; *de Viron et al.*, 2001b]. In contrast, however, several studies have noted the absence of any robust ENSO signature in geodetic records of polar motion [cf. *Chao and Zhou*, 1999, and references therein]. The ENSO being a strong global mode of the atmosphere implies a robust effect on Earth-atmosphere interaction, and strong axial atmospheric torques have been associated with the large LOD changes seen during different phases of the ENSO cycle [*Ponte and Rosen*, 1999; *de Viron et al.*, 2001b]. This paper addresses the following questions: what are the characteristics of the equatorial atmospheric torques during the ENSO cycle, and why do they appear to have no detectable effect on the observed polar motion?

[6] As the ENSO is an interannual mode, it is possible to approximate the ocean response to the atmospheric pressure forcing by using the inverted barometer (IB) assumption. In section 2, we describe this approximation and explain how the torque evaluation can be adapted in the frame of this method. This approximation is used in the following sections. In section 3, we discuss the interaction between the Earth and its atmosphere related to the El Niño; we explain why, whereas the atmosphere's dynamics are deeply affected by the ENSO cycle, there is little consequent effect that can be observed in the polar motion. Section 4 is devoted to conclusions.

2. IB Torques

[7] The principle of the IB approximation is to obtain, from atmospheric data only, a good representation of the combined mass loading effect of the atmosphere and the atmospheric pressure-forced ocean [e.g., *Jeffreys*, 1915]. We assume that the ocean responds quasi-statically to the atmospheric pressure forcing at long time scales, i.e., the water height drops where the pressure is high and rises where it is low, so that the total pressure is the same at all the points of the same depth. A classical application is the IB AAM, computed routinely from operational model output in order to monitor the atmospheric effect on Earth rotation. Let us define the IB pressure as equal to the atmospheric surface pressure over land areas and the average surface pressure (computed for the whole world ocean) over ocean areas. The IB AAM is then computed using the wind as usual for the motion term and the IB pressure for the matter term. In order to compute the corresponding atmospheric torque, we have to define the equivalent of the IB hypothesis in terms of a correction to the standard torque calculation methods [cf. *de Viron et al.*, 2001a, and references therein].

2.1. Mountain and Ellipsoidal Torques

[8] The mountain and ellipsoidal torques may be computed directly from the IB pressure, using the standard techniques referenced above. As the oceanic pressure is assumed to be uniform at a given (geopotential) depth, only the land areas can generate a net orographic pressure torque on the solid Earth. Consequently, the mountain torque calculation is not affected by the IB hypothesis, since for these purposes the ocean surface is considered to be "flat." Conversely, the ellipsoidal torque is computed using the pressure loading on the (2,0) spherical harmonic or "centrifugal" component of the Earth's topography, and the IB assumption must be used to obtain the correct net torque over ocean-covered areas.

2.2. Friction Torques

[9] Here two different cases can occur: the IB approximation can be used together with a nonpressure forced ocean model, which includes the wind friction forcing of the ocean, or it is used with no ocean data. If an ocean model is used together with the IB approximation to directly compute the effect of surface wind forcing on ocean-solid Earth torques, then the atmospheric friction torque on the solid Earth is to be computed over the land area only. As explained above, the friction torque is computed from the surface wind stress obtained from atmospheric GCMs. If no ocean model is used, we can adapt the torque computation by assuming that angular momentum lost or gained by the atmosphere over the ocean has been transmitted to the solid Earth, through some adjustment process. Consequently, the effective friction torque in this case has to be computed from the atmospheric surface stress acting over the whole Earth.

2.3. Dissipation Torques

[10] As the IB ocean adjusts to atmospheric loading, the change in its angular momentum in the rotating frame exactly compensates the non-IB changes in the AAM matter term,

$$\Delta \vec{O}^{\mathrm{IB}} = \Delta\left(\vec{H}_{\mathrm{M}}^{\mathrm{non-IB}} - \vec{H}_{\mathrm{M}}^{\mathrm{IB}}\right), \tag{1}$$

where $\vec{H}_{\mathrm{M}}$ is the matter term of the angular momentum and $\vec{O}$ is the total angular momentum of the oceans. Whereas frictional atmospheric stresses on the ocean are accounted for in the angular momentum budget as described above, however, atmospheric pressure on the "flat" ocean surface is associated with no explicit torque, and hence the net angular momentum of the IB ocean does not change as the atmospheric loading varies. Non-IB changes in the atmospheric matter term must then be balanced by Coriolis torques, associated with the

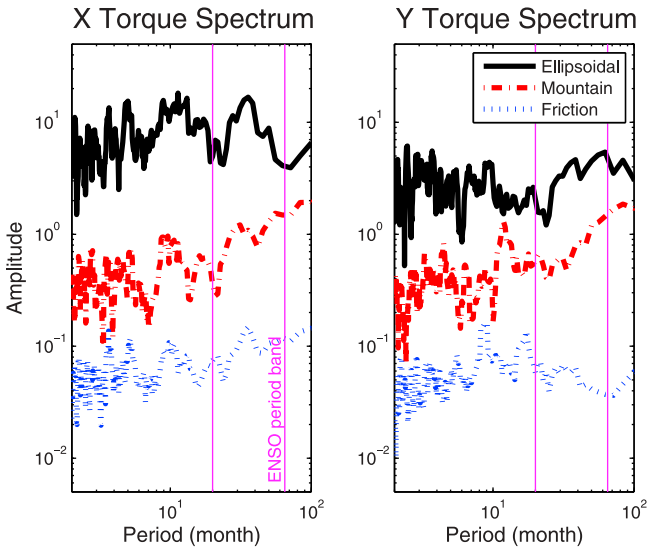

Figure 1. Fourier amplitude spectrum of the torque. Note the logarithmic scale.

oceanic mass motions induced by time-variable atmospheric loading in the rotating frame,

$$\vec{\Gamma}_{\mathrm{Cor}} = \frac{\partial}{\partial t}\vec{O}^{\mathrm{IB}}. \tag{2}$$

We may treat this torque on the IB ocean in a similar manner to the atmospheric friction torque by assuming that it is rapidly transmitted by an adjustment process to the solid Earth, which then exerts an effective "dissipation" torque on the ocean given by

$$\vec{\Gamma}_{\mathrm{Dissipation}} = \frac{\partial}{\partial t}\left(\vec{H}_{\mathrm{M}}^{\mathrm{IB}} - \vec{H}_{\mathrm{M}}^{\mathrm{non-IB}}\right), \tag{3}$$

with $\vec{\Gamma}_{\mathrm{Dissipation}}$, the dissipation torque, also being computed in the rotating frame. This definition of the dissipation torque is logical from both the physical and the mathematical point of view, since it ensures the conservation of angular momentum in the IB case if the non-IB case is conserved. In particular, the angular momentum budget equation for the atmosphere and ocean system can be written as

$$\frac{\mathrm{d}\vec{H}^{IB}}{\mathrm{d}t} = \vec{\Gamma}^{\mathrm{IB}}_{\mathrm{Ellipsoidal}} + \vec{\Gamma}_{\mathrm{mountain}} + \vec{\Gamma}^{\mathrm{IB}}_{\mathrm{Friction}} + \vec{\Gamma}^{\mathrm{IB}}_{\mathrm{Dissipation}}, \tag{4}$$

with the IB superscript indicating that the quantity is modified in the frame of the IB approximation, and the derivative is taken in the nonrotating frame.

3. Earth-Atmosphere Interaction During the ENSO

[11] The ENSO is a global scale oscillation of the ocean/atmosphere system. Consequently, one would expect it to affect the Earth-ocean and Earth-atmosphere rotational interaction to an observable level; in particular, this should lead to a noticeable polar motion associated with ENSO events. Several previous studies have looked for a correlation between atmospheric excitation of polar motion and the ENSO cycle but have found that, under the IB assumption, it was very marginal and/or not significant [e.g., *Abarca del Rio and Cazenave*, 1994; *Chao and Zhou*, 1999]. Those studies searched for an ENSO signature in the angular momentum budget of the Earth by investigating the relationship between the equatorial components of AAM and the Southern Oscillation Index (SOI). In this paper, we use a different approach by directly analyzing equatorial components of the Earth-atmosphere torques associated with El Niño. The IB assumption is used, as the involved time scale is (by far) long enough to justify a static approximation for the ocean response. This allows us to focus attention on the atmospheric dynamical contribution to polar motion during the ENSO cycle.

3.1. Data and Methods

[12] In order to analyze atmospheric torques associated with ENSO, we use surface wind and pressure data from the National Centers for Environmental Prediction/National Center for Atmospheric Research (NCEP/NCAR) reanalysis [*Kalnay et al.*, 1996], averaged to form monthly time series. The state of the ENSO cycle is monitored using the Southern Oscillation Index (SOI), constructed as the normalized surface pressure difference between Darwin, Australia, and Tahiti; these values are given as a monthly time series by the NCAR Climate Analysis Section. The appropriate geodetic excitation functions (described further below) were obtained as monthly values from the International Earth Rotation Service (IERS). All series were analyzed for the 42 year period 1968–2009; earlier reanalysis data were found to have deficiencies in the representation of atmospheric torques and so were not considered in this study. In what follows, spectra and coherence were computed from Fourier transforms of the data using a Hanning (10% split-cosine taper) window with 11-point frequency domain smoothing, giving approximately 20 equivalent degrees of freedom [cf. *Bloomfield*, 2000] for each of the estimates shown in Figures 1 and 2. Prior to the frequency domain analysis, a composite seasonal cycle and secular trend were removed from each of the time series considered.

3.2. Equatorial Torques and the SOI

[13] Figure 1 shows the spectrum of the three components of the torque (ellipsoidal, mountain, and friction) as a function of the period (note the logarithmic scale). Since the Earth's departure from sphericity (amplitude 21 km) is roughly an order of magnitude larger than its typical surface orography, the equatorial torque is expected to be dominated by the effect of the Earth's bulge (i.e., the ellipsoidal torque), representing the combined action of the atmospheric pressure "pushing" on the bulge and the gravitational attraction of the bulge by the air mass anomalies. The results presented here show that while the ellipsoidal torque dominates for the X component at monthly and longer periods, the *Y* component of the mountain torque may not be negligible compared to the IB bulge torque for seasonal to interannual periods. Unlike the case for axial atmospheric torques, the equatorial components of the friction torque are substantially weaker than the corresponding components of the mountain torque for monthly to interannual periods. As expected, the dissipation torques (not shown), introduced to provide closure of the IB-AAM budget,

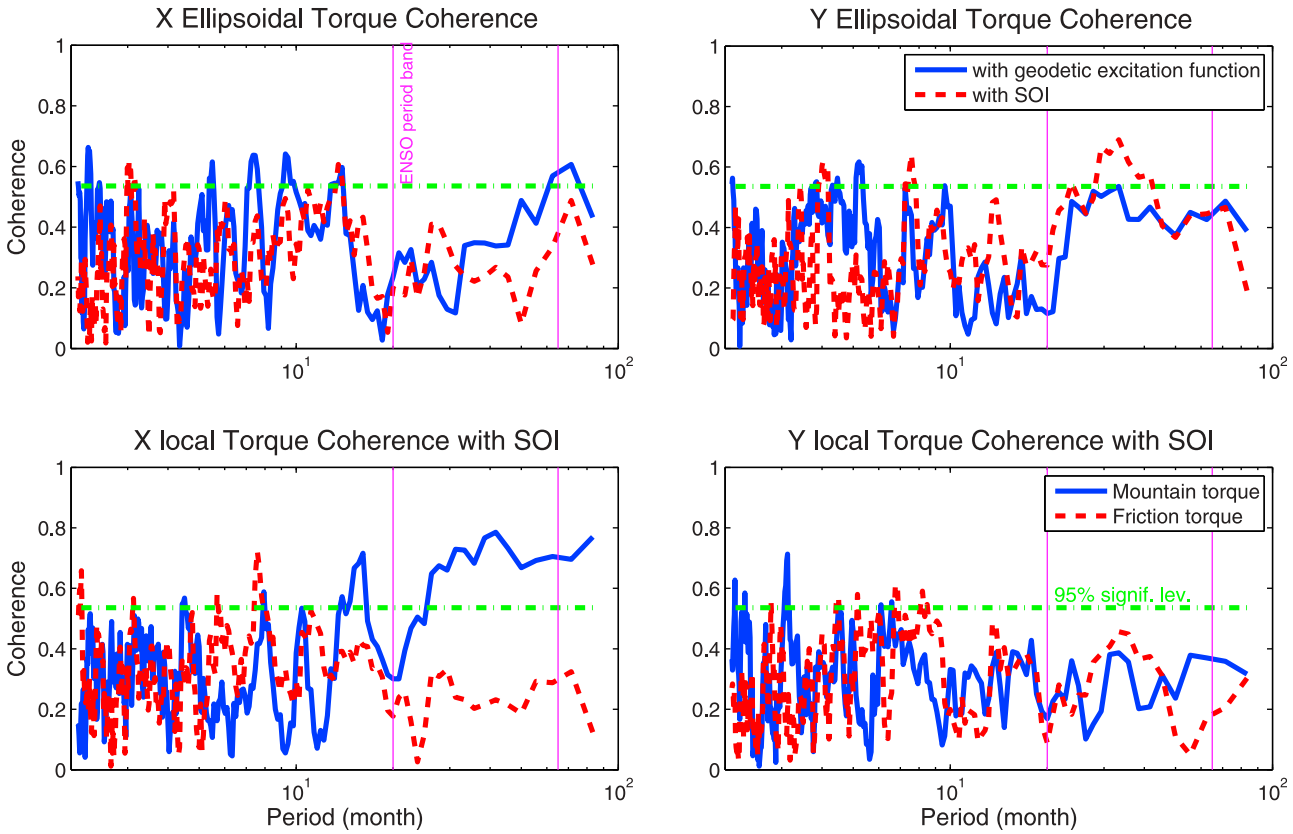

Figure 2. Coherence of the torque with the SOI. (top) Coherence of the ellipsoidal torque with the geodetic excitation and with the SOI. (bottom) Coherence of the local torque (mountain and friction) with the SOI.

are quite small on these time scales and will not be further considered.

[14] In order to investigate atmospheric effects on polar motion associated with the ENSO cycle, we consider separately the ellipsoidal torques and the equatorial "local" (mountain and friction) torques. In the two top frames of Figure 2, we show the coherence between the SOI and the X and Y components of the ellipsoidal torque (red curves). It can be observed that the coherence reaches the 95% significance level for the Y component in the ENSO band, while the X component of the ellipsoidal torque shows no significant coherence with the SOI. The smaller overall amplitude for the Y torque (Figure 1), however, resulting from its greater dependence on contributions from pressure variations over the oceans, which are reduced by the isostatic IB correction, limits its geodetic signature (see further discussion below).

[15] The blue curves in the upper plots show the coherence with the geodetic excitation function for the two ellipsoidal components. Those functions, as defined by *Munk and MacDonald* [1960], express what the excitation should be in order to explain the observed polar motion. This formalism effectively deconvolves the Chandler Wobble resonance from the observed polar motion [cf. *Jeffreys*, 1939]. It can be seen that the atmospheric ellipsoidal torque is only marginally coherent with the excitation, meaning that other sources need to be considered on these time scales, in particular the ocean and land hydrology [e.g., *Gross et al.*, 2003; *Jin et al.*, 2010]. Interestingly, however, the X component of the mountain torque, with interannual amplitude only slightly less than the Y ellipsoidal torque, shows high coherence with the SOI, which results from the interaction of ENSO-related atmospheric pressure anomalies with large-scale orographic features, as discussed below.

3.3. Ellipsoidal Torques

[16] It could seem surprising, considering the large atmospheric pressure anomaly associated with the ENSO, that the corresponding ellipsoidal torque is not strong enough to generate an observable polar motion. The reason is largely geometrical: the ellipsoidal torque is associated with surface pressure loading corresponding to the spherical harmonics of degree 2, order 1, which divide the world into four subregions. The contributions from the different parts of the world tend to cancel each other out, which provides a globally smaller total torque. The IB effect of the oceans also plays an important role in reducing the atmospheric loading effect on the ellipsoidal torque, as discussed below. The local covariance of the surface pressure with the SOI is shown in Figure 3a; a delay of 3 months has been applied to the pressure field in this and subsequent covariance calculations to allow for the large-scale response time of the atmosphere to ENSO-related SST changes [cf. *Dickey et al.*, 2007, and references therein]. Interestingly the major continental systems, including Asia, North America, and Australia, all show negative covariance with the SOI (i.e., they tend to have higher pressure during El Niño).

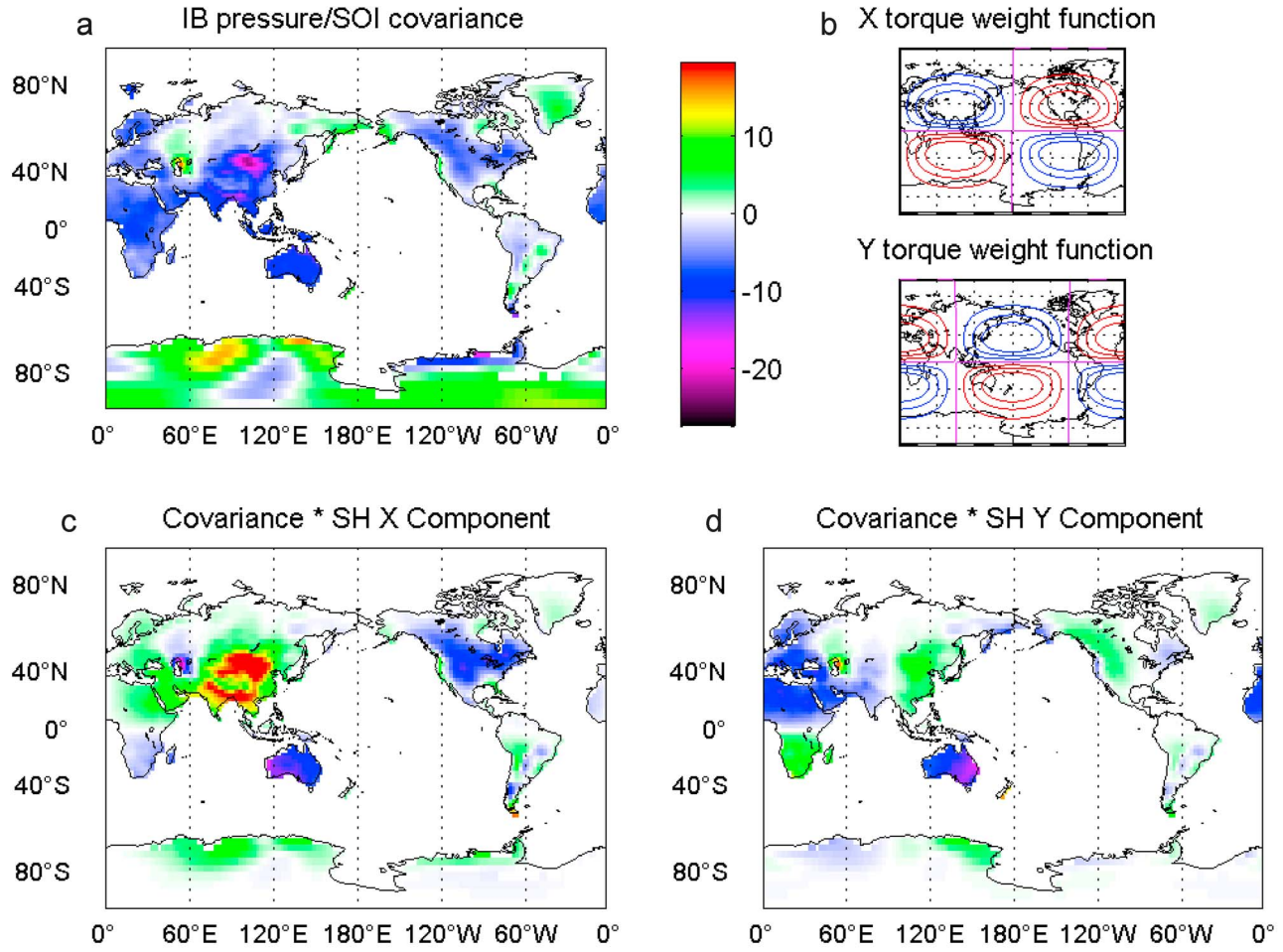

Figure 3. (a) Covariance of the surface pressure with the SOI (delayed by 3 months), in units of hPa (see color bar). (b) The 2,1 spherical harmonic weight functions used to compute the ellipsoidal torques by global integration with the IB pressure; red and blue contours denote positive and negative values, respectively. (c and d) The resulting ellipsoidal torque covariance with the SOI for the *X* and *Y* components respectively, in equal arbitrary units scaled to optimize contrast within the Figure 3a color bar.

[17] To compute the *X* and *Y* components of the ellipsoidal torque, we form global integrals of the surface pressure, area-weighted by the spherical harmonics (SH) of degree 2, order 1, which are illustrated in Figure 3b (top) and 3b (bottom), respectively. For the *X* component, in particular, extrema of the 2,1 SH pattern coincide with the major continental areas of Asia and North America, with portions of Australia and South America also heavily weighted. Because of the largely negative covariance of the surface pressure with the SOI over these areas noted in Figure 3a, therefore, the contributions to the *X* ellipsoidal torque covariance from the four subregions of the 2,1 SH pattern tend to have a canceling effect. This is illustrated in Figure 3c, where positive ellipsoidal torque contributions from Asia and South America are seen to be counterbalanced by negative contributions from North America and Australia. This effect is quantitatively documented in Table 1, which shows the resulting torque-SOI covariances integrated over the individual subregions and globally, where A or B refer to west or east, respectively, and 1 or 2 refer to north or south. Interestingly, the total torque covariance for the *X* component is seen to be less than half of its positive value over the Asian quadrant, illustrating the canceling effect of the 2,1 *X* component on the SOI covariant pressure loading pattern.

[18] For the *Y* torque, by contrast, the extrema of the 2,1 SH pattern are mostly located over the oceans; because of the action of the IB effect, therefore, the covariances in the individual subregions are generally smaller than their *X*

Table 1. Covariance of the SOI With the X and Y Components of the Ellipsoidal Torque, for the Quadrants Shown in Figure 3b and Globally[a]

	X	*Y*
A1	9.756	−6.334
B1	−2.183	0.931
A2	−2.975	1.031
B2	0.243	−2.904
Global	4.841	−7.276

[a]For the *X* component, A and B refer to west or east, respectively, and 1 and 2 refer to north and south; for the *Y* component, A refers to the quadrants centered on the Greenwich meridion, while B refers to quadrants centered on the date line. Units are Hadleys (10^{18} Nm).

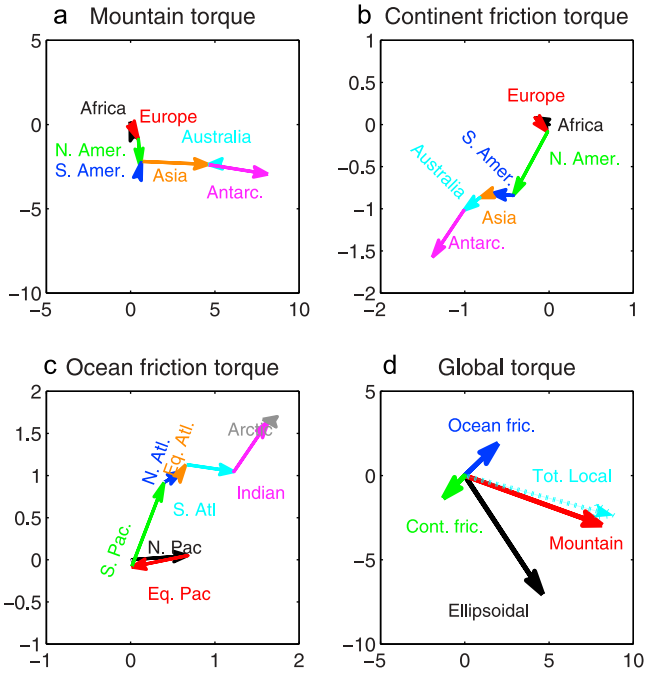

Figure 4. Phase diagram of the covariance of the local torque with the SOI, by (a and b) continent and (c) ocean basin, and of (d) the total local and ellipsoidal torques. Units are 10^{18} Nm, with the X and Y components given by the horizontal and vertical axes, respectively. Note that the scales are different for each graph.

torque counterparts (Table 1; note that A here refers to the quadrants centered on the Greenwich meridian, while B refers to quadrants centered on the date line). In this case however, the largest (negative) contributions from Europe-North Africa and Australia tend to reinforce each other (Figure 3d), so that the global covariance magnitude with the SOI is actually somewhat larger than for the X component (Table 1). It is interesting to note that Australia, containing one of the pressure centers of the SOI (Darwin) and located on the eastern (western) end of a positive lobe of the X component (Y component) weighting pattern, makes a similar negative contribution to both torque covariances (subregions A2 for the X component and B2 for the Y component).

3.4. Local Torques

[19] As explained in the section 2, the torque under the IB hypothesis is composed of four parts: the ellipsoidal torque, the mountain torque, the friction torque, and the dissipation torque. In the case of the equatorial torque, the dissipation torque is negligible; this is due to the large value of the ellipsoidal (and to some extent of the mountain) torque at low frequency (see Figure 1). In Figure 4, we show the contribution from the different continents and ocean basins (color arrows), computed as the covariance of the regional torque with the SOI. For example in Figure 4a, it can be seen that the ENSO-related mountain torques from Africa, Europe, and the Americas are strongest in the Y component, while the contributions from Asia, Antarctica, and Australia are dominated by the torques in the X direction. For Figures 4a–4c, the resulting regional torque vectors are plotted sequentially (nose to tail), so that the position of the final end-point corresponds to the net torque covariance with the SOI for that quantity (e.g., mountain torque in Figure 4a), relative to the origin (0,0 point) in each frame. For purposes of intercomparison, each of the total torque covariances from Figures 4a to 4c is plotted relative to the origin in Figure 4d, along with their sum and the ellipsoidal torque covariance (taken from bottom row of Table 1). Note that the ENSO-related ocean and continental friction torques are quite small and are almost opposite to each other, so that the net local response (denoted by the dashed cyan arrow in Figure 4d) is due almost entirely to the mountain torque (red arrow in Figure 4d).

[20] As found by *de Viron et al.* [2001a] for solar (diurnal) tidal forcing, the ENSO-related equatorial mountain torque is mainly generated over Asia (i.e., the Himalayas) and Antarctica (Figure 4a); the Andes do not contribute so much due to their equatorial position and north-south orientation. The large effect of the Antarctica can be better understood by looking at the pressure anomaly around this continent (Figure 5). An area of strong negative covariance with the SOI, resembling the ENSO-driven Pacific-South American mode [e.g., *Mo and Paegle*, 2001; *Fogt and Bromwich*, 2006] is centered at the western approaches to the Drake Passage, interacting with both the South American and Antarctic continents (Figure 5a). While most orographic features have height gradients of opposite sign located within relatively short distances [*de Viron et al.*, 2001a, Plate 4], the greater extent of the Antarctic continent allows large-scale pressure gradients to couple more efficiently with the orography (Figure 5b). It can also be observed that the pressure loading on Antarctica mainly affects the X mountain torque (straight black line), consistent with the predominantly zonal orientation of the Antarctic pressure torque covariance with the SOI (magenta arrow in Figure 4a).

4. Concluding Remarks

[21] The ENSO cycle is one of the most important signals in the dynamics of the atmosphere. It has been known for many years that it has an observable effect on LOD variations. Nevertheless, several studies have shown that there is little significant associated effect on the polar motion. In this study, we investigate this problem from the point of view of the torques, which couple the atmosphere with the solid Earth. We find that, unlike the polar motion, the interaction torques between the atmosphere and the solid Earth do show unambiguous ENSO signatures: The Y component of the ellipsoidal torque and the X component of the mountain torque are both highly correlated with the SOI in the ENSO band (see Figure 2). Nevertheless, they fail to generate a significant PM response to ENSO. As discussed in section 3.3, the magnitudes of the SOI-related ellipsoidal torques are mitigated by geometrical factors, as both components (X and Y) are associated with degree 2 order 1 SH components of the pressure distribution. For the largely land-based X component, the similar pressure covariance with the SOI over the major continents (Figure 3a) results in partial cancellation of the torque contributions obtained by area-weighted integration with the appropriate 2,1 SH (Figure 3c). The ellipsoidal Y torque, with most of its weighting pattern located over the oceans, is itself limited in amplitude by the IB effect, which tends to spread the loading anomalies across the alternating

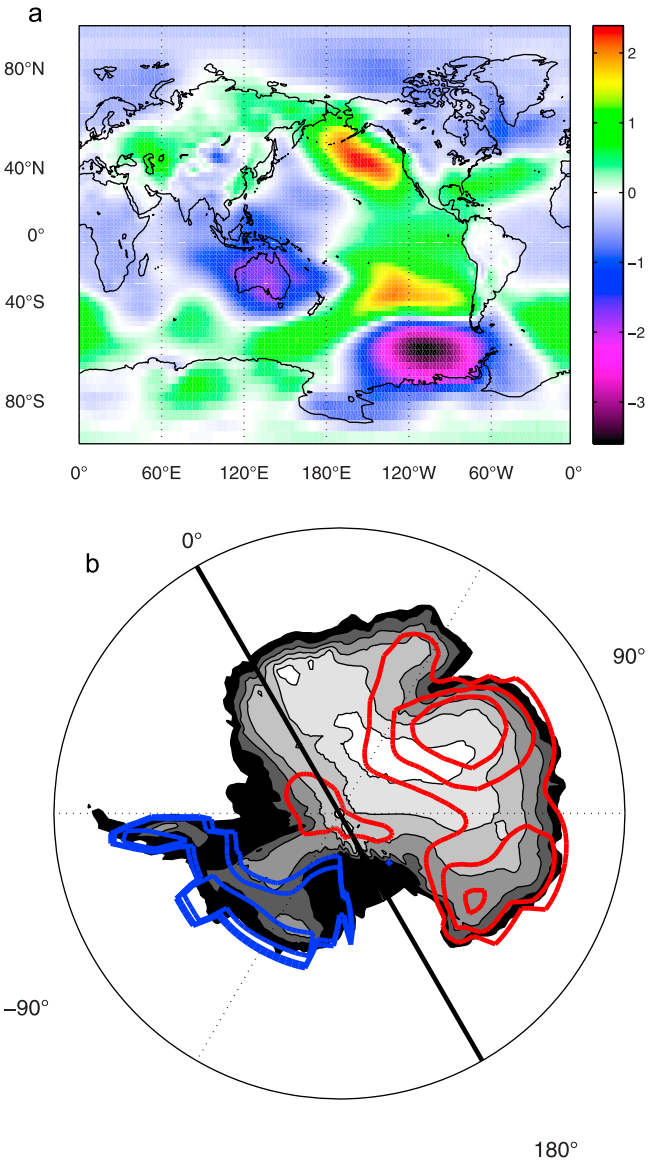

Figure 5. (a) Surface pressure covariance with the SOI; units are hPa. The large negative anomaly in the western approaches to the Drake Passage is representative of the Pacific-South America mode response to ENSO. (b) Antarctic land surface pressure covariance with the SOI; units are hPa. The gray shading represents orography, and the red (blue) contours denote covariances of plus (minus) 0.3, 0.5, and 1.0 hPa. Note that the Antarctic pressure gradient is mainly in the *Y* direction, giving a torque predominantly in the *X* direction (straight black line) on a rotating planet.

sign pattern of the appropriate 2,1 SH (Figure 3d). The resulting isostatic pressure correction over the oceans leads to substantial mitigation of the torque, which would be generated by direct interaction of the ENSO-induced atmospheric pressure anomalies (Figure 5a) with the solid Earth.

[22] Classically [see *Bell*, 1994], one expects the equatorial atmospheric torques to be dominated by the bulge effect, but due to the roughly symmetrical land-based and IB ocean-based pressure loading response to ENSO, both the *X* and *Y* components of the ellipsoidal torques are reduced to amplitudes comparable to the sum of the local torques (Figure 4d). While the friction and dissipation torques are found to be negligible on these time scales, the *X* component of the mountain torque shows a large covariance with the SOI (Figure 4a), mostly due to the action of ENSO-related pressure differences acting over the Himalayas and Antarctica (see Figure 5). Consequently, the study of the dynamics of low-frequency equatorial atmospheric angular momentum needs to include the mountain torque, in particular the interaction of teleconnected surface pressure anomalies with the Asian and Antarctic continents. Full elucidation of the PM effects associated with ENSO will require consideration of oceanic and land hydrological processes as well.

[23] **Acknowledgments.** This paper presents the results of one phase of research carried out at the Jet Propulsion Laboratory, California Institute of Technology, sponsored by the National Aeronautics and Space Administration. The contribution of OdV to this study is IPGP contribution 3062.

References

Abarca del Rio, R., and A. Cazenave (1994), Interannual variations in the Earth's polar motion for 1963–1991: Comparison with atmospheric angular momentum over 1980–1991, *Geophys. Res. Lett.*, *21*(22), 2361–2364, doi:10.1029/94GL02285.

Barnes, R. T. H., R. Hide, A. A. White, and C. A. Wilson (1983), Atmospheric angular momentum fluctuations, length-of-day changes and polar motion, *Proc. R. Soc. Lond., Ser. A*, *387*, 31–73.

Bell, M. J. (1994), Oscillation in the equatorial components of the atmosphere angular-momentum and torques on the Earth's bulge, *Q. J. R. Meteorol. Soc.*, *120*, 195–213.

Bloomfield, P. (2000), *Fourier Analysis of Time Series*, 261 pp., John Wiley, New York.

Chao, B. F. (1989), Length-of-day variations caused by El-Nino–Southern Oscillation and Quasi-Biennial Oscillation, *Science*, *243*, 923–925.

Chao, B. F., and Y. H. Zhou (1999), Meteorological excitation of interannual polar motion by the North Atlantic Oscillation, *J. Geod.*, *27*, 61–73.

Chen, J. L., C. R. Wilson, B. F. Chao, C. K. Shum, and B. D. Tapley (2000), Hydrologic and oceanic excitations to polar motion and length-of-day variation, *Geophys. J. Int.*, *141*, 149–156.

de Viron, O., C. Bizouard, D. Salstein, and V. Dehant (1999), Atmospheric torque on the Earth and comparison with atmospheric angular momentum variations, *J. Geophys. Res.*, *104*(B3), 4861–4875, doi:10.1029/1998JB900063.

de Viron, O., S. L. Marcus, and J. O. Dickey (2001a), Diurnal angular momentum budget of the atmosphere and its consequences for Earth's nutation, *J. Geophys. Res.*, *106*(B11), 26,747–26,759, doi:10.1029/2000JB000098.

de Viron, O., S. L. Marcus, and J. O. Dickey (2001b), Atmospheric torques during the winter of 1989: Impact of ENSO and NAO positive phases, *Geophys. Res. Lett.*, *28*(10), 1985–1988, doi:10.1029/2000GL012675.

Dickey, J. O., S. L. Marcus, and R. Hide (1992), Global propagation of interannual fluctuations in atmospheric angular momentum, *Nature*, *357*, 484–488.

Dickey, J. O., S. L. Marcus, and T. M. Chin (2007), Thermal wind forcing and atmospheric angular momentum: Origin of the Earth's delayed response to ENSO, *Geophys. Res. Lett.*, *34*, L17803, doi:10.1029/2007GL030846.

Fogt, R. L., and D. H. Bromwich (2006), Decadal variability of the ENSO teleconnection to the high-latitude South Pacific governed by coupling with the Southern Annular Mode, *J. Clim.*, *19*, 979–997.

Gross, R. S., I. Fukumori, and D. Menemenlis (2003), Atmospheric and oceanic excitation of the Earth's wobbles during 1980-2000, *J. Geophys. Res.*, *108*(B8), 2370, doi:10.1029/2002JB002143.

Jeffreys, H. (1915), Causes contributory to the annual variation of latitude, *Mon. Not. R. Astron. Soc.*, *76*, 499–528.

Jeffreys, H. (1939), The variation of latitude, *Mon. Not. R. Astron. Soc.*, *100*, 139–155.

Jin, S., D. P. Chambers, and B. D. Tapley (2010), Hydrological and oceanic effects on polar motion from GRACE, *J. Geophys. Res.*, *115*, B02403, doi:10.1029/2009JB006635.

Kalnay, E., et al. (1996), The NCEP/NCAR 40-year reanalysis project, *Bull. Am. Meteorol. Soc.*, *77*, 437–471.

Marcus, S. L., O. de Viron, and J. O. Dickey (2004), Atmospheric contributions to Earth nutation: Geodetic constraints and limitations of the torque approach, *J. Atmos. Sci.*, *61*, 352–356.

Mo, K. C., and J. N. Paegle (2001), The Pacific-South American modes and their downstream effects, *Int. J. Climatol.*, *21*, 1211–1229.

Munk, W. H., and G. J. F. MacDonald (1960), *The Rotation of the Earth: A Geophysical Discussion*, 323 pp., Cambridge Univ. Press, New York.

Ponte, R. M., and R. D. Rosen (1999), Torques responsible for the evolution of atmospheric angular momentum during the 1982–83 El Niño, *J. Atmos. Sci.*, *56*, 3457–3462.

Ponte, R. M., and D. Stammer (2000), Global and regional axial ocean angular momentum signals and length-of-day variations (1985–1996), *J. Geophys. Res.*, *105*(C7), 17,161–17,171, doi:10.1029/1999JC000157.

Rosen, R. D., D. A. Salstein, T. M. Eubanks, J. O. Dickey, and J. A. Steppe (1984), An El Niño signal in atmospheric angular momentum, *Science*, *225*, 411–414.

Wahr, J. M. (1982), The effects of the atmosphere and oceans on the Earth's wobble: I. Theory, *Geophys. J. R. Astron. Soc.*, *70*, 349–372.

O. de Viron, University Paris Diderot and Institut de Physique du Globe de Paris (CNRS), Paris 75005, France.

J. O. Dickey and S. L. Marcus, Jet Propulsion Laboratory, California Institute of Technology, Pasadena, CA 91109, USA.